Zigzag Morphology of a Poly(styrene-*b*-hexyl isocyanate) Rod–Coil Block Copolymer

J. T. Chen and E. L. Thomas*

Department of Materials Science and Engineering, Massachusetts Institute of Technology, Cambridge, Massachusetts 02139

C. K. Ober* and S. S. Hwang†

Department of Materials Science and Engineering, Cornell University, Ithaca, New York 14853

Received July 22, 1994; Revised Manuscript Received November 14, 1994®

ABSTRACT: The solid state morphology of an anionically synthesized P(S-*b*-HIC) rod–coil block copolymer was studied using a number of techniques and casting solvents. Liquid crystalline ordering was seen in concentrated solutions using optical microscopy (OM). Bulk and thin film samples cast from solutions in toluene and studied using transmission electron microscopy (TEM) revealed a new zigzag morphology. Electron diffraction (ED) experiments were able to show that the PHIC rods were tilted with respect to the interface separating the PS and PHIC domains. In addition, the PHIC rods were found to be highly crystalline, having an 8_3 or 8_5 helical conformation and packing in a two chain monoclinic or triclinic (pseudohexagonal) unit cell with $a = b = 15.1$ Å, $c = 15.6$ Å, $\gamma = 120°$, and a crystal density of 1.10 g/cm^3. A model for the zigzag morphology which allows interdigitation of the rods is consistent with TEM and ED results as well as domain spacing predictions based on molecular weight information. The formation of such a morphology is also consistent with thermodynamic arguments based on a theory developed by Halperin for rod–coil block copolymers if, in addition, quantization of the allowed tilt angle by crystallization is taken into account. Solvent quality was found to profoundly affect the morphology formed from solution cast samples. In addition to the zigzag morphology, morphologies consisting of fragmented PS zigzags and micelle-like regions were also observed. The choice of solvent most likely determines what phases macrophase separate from the isotropic solution before microphase separation of the rod–coil and crystallization of the PHIC take place and also whether chain stretching or interfacial energy is more dominant in the thermodynamics of microphase separation.

I. Introduction

The morphology and phase behavior of AB diblock copolymers consisting of two flexible blocks have been extensively studied both experimentally[1–6] and theoretically[7–14] and are relatively well understood. Coil–coil diblocks have been found to exhibit a wide range of microphase-separated morphologies due to the mutual repulsion of the dissimilar blocks and the constraints imposed by the connectivity of the A and B blocks. The parameters which determine the resulting morphology of a given block copolymer[12] are the Flory–Huggins interaction parameter, χ_{AB}, the total degree of polymerization, $N = N_A + N_B$, and the volume fraction of the A component, f_A. However, most AB diblock copolymers can better be described as flexible–semiflexible block copolymers due to conformational asymmetry caused by differences in the statistical segment length of each block. Recent theoretical attempts[15–17] have been made to deal with this conformational asymmetry and study its effects on the microphase-separated morphologies. Increasing the chain stiffness of a polymer chain eventually results in a rigid rodlike molecule which can be characterized by a persistence length, L, and whose end-to-end distance scales linearly with the number of monomer units. Rodlike polymers have been widely studied and found to exhibit liquid crystalline ordered phases in solution[18] in which the molecules are oriented along a preferred direction described by the director $\hat{\mathbf{n}}$. For these polymers, the relevant factors which influence the formation of a liquid crystalline phase are temperature and solvent concentration. AB diblock copolymers consisting of a flexible coil block and a rigid rod block, hereafter called rod–coil block copolymers, represent the extreme case in conformational asymmetry. The driving forces controlling the microphase separation behavior of rod–coil block copolymers are expected to be quite different from traditional flexible block copolymers due to the mesogenic nature of the rod block.

In comparison to the numerous studies on coil–coil diblock copolymers and liquid crystalline polymers, only a few studies of the microphase separation characteristics of rod–coil block copolymers have been performed in recent years. Experimentally, rod–coil diblock copolymers with polypeptide rod blocks were the first type synthesized. All samples were found to exhibit a lamellar morphology.[19–23] In addition, one of the studies[22] that involved hydrophobic–hydrophilic polypeptide rod–coil block copolymers with coil volume fractions ranging between approximately 25 and 40% showed that the rods were tilted 15–70° in the lamellae and that the tilt angle increased with water content. In all of these studies, the rodlike polypeptide chain had an α-helical confirmation. Polypeptides, however, can also undergo various types of folding and are difficult to synthesize with narrow molecular weight distributions, making them less attractive as rod–coil materials. More recently, a low molecular weight monodisperse rod–coil diblock was synthesized[24] and found to exhibit a lamellar morphology after annealing. Significant theoretical work on rod–coil systems has lagged experimental studies for the most part. The earliest theories[25,26] of rod-coil diblock copolymers predicted nematic–smectic A and smectic A–smectic C transi-

* Authors for correspondence.
† Present address: Polymer Processing Laboratory, Korean Institute for Science and Technology, P.O. Box 131, Cheongryang, Seoul, Korea.
® Abstract published in *Advance ACS Abstracts,* February 1, 1995.

0024-9297/95/2228-1688$09.00/0

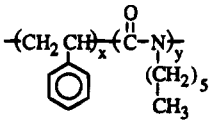

P(S-b-HIC)

Figure 1. Chemical formula of the poly(styrene-*b*-hexyl isocyanate), P(S-*b*-HIC), rod–coil diblock copolymer. PS is the flexible coil block, and PHIC, the rigid rod block. Due to an inherent chain stiffness, PHIC adopts an α helical conformation. For the sample studied $x \approx 300$ and $y \approx 900$.

tions in the melt and in solutions of a solvent preferential to the coil block. Other theoretical work[27,28] has dealt more with the aggregation behavior and phase behavior of rod–coil diblocks in a solvent preferential for the coil. These studies have predicted, not only the familiar lamellar phase but also, for sufficiently low χ_{AB} and a large coil volume fraction, various "hockey puck" micelle phases. Theoretical treatments of flexible–rigid–flexible triblock copolymers[29,30] have also predicted "fence" and "needle" morphologies. Clearly, more systematic experimental studies involving better model systems are needed to fully understand the complete range of morphologies formed by rod–coil diblock copolymers and to test some of the existing theories.

This paper presents a study of the morphology of a novel high molecular weight anionically synthesized rod–coil diblock copolymer having a polystyrene (PS) coil block and a poly(hexyl isocyanate) (PHIC) rod block. The solvents employed are toluene, CCl_4, and $CHCl_3$. Previous X-ray diffraction work[31] on drawn PHIC samples concluded that PHIC adopts a 12_5 helix conformation and is crystalline in the solid state. Experimental studies on the solution behavior of polyisocyanates[32,33] have shown that PHIC is a stiff rod in a wide range of solvents including those used in this study and has a persistence length of about 500–600 Å. The inherent chain stiffness of PHIC is primarily due to short range restrictions to rotation and is unaffected by long range forces, which is consistent with the helical nature of the PHIC. $CHCl_3$, however, is known to exhibit a solvent–solute interaction which alters the barriers to rotation, resulting in a slightly altered conformation for PHIC. In addition, the lyotropic behavior of PHIC in a number of different solvents has been confirmed and extensively studied.[34–36] Optical microscopy under crossed polarizers of several PHIC solutions showed that above a certain concentration v_c, the solutions phase separated into a solvent rich isotropic phase and a PHIC rich anisotropic nematic phase. In the optically birefringent anisotropic domains, the PHIC molecules are oriented along a preferred direction described by the local director. For PHIC homopolymers with molecular weights between 65 000 and 75 000, v_c varied between 15 and 25 wt % for different solvents and decreased with increasing molecular weight.[34,35]

II. Synthesis of Poly(styrene-*b*-hexyl isocyanate)

A rod–coil diblock copolymer having a PS coil block and a PHIC rod block (see Figure 1) was synthesized using anionic polymerization techniques. To begin, the solvents THF and toluene were rigorously dried. Styrene monomer was distilled over CaH_2 and stirred over dibutylmagnesium for 12 h. The hexyl isocyanate monomer was stirred for 1 day over Et_3Al. After drying, the styrene and hexyl isocyanate monomer were transferred by vacuum distillation to monomer port 1 and monomer port 2 of the reactor, respectively. An *n*-Butyllithium solution (0.2 mL) (1.6 M in hexane) was added to the reaction flask which was evacuated for 2 h after cooling to −78 °C using a dry ice/2-propanol bath. Dry THF (150 mL) and toluene (250 mL) were added to the reactor via vacuum distillation. Monomer port 1 of the reactor was opened, and styrene monomer (3 g) was added to begin the polymerization. The polymerization was then allowed to proceed at −78 °C for 24 h. At this point, hexyl isocyanate monomer (27 g) was added to the reactor by opening monomer port 2 of the reactor. Formation of the hexyl isocyanate block was allowed to proceed at −78 °C for 2 h at which point 1.5 mL of methanol was added to terminate the polymerization. The resulting polymer was precipitated in 2 L of MeOH, filtered out, and dried. The reaction yielded ~6 g of polymer. NMR and GPC were performed to determine the molecular weight and composition of the block copolymer. GPC was performed using a UV (254 nm) detector and a refractive index detector and indicated that the rod–coil has a uniform composition. Ultrastyragel columns of 500, 1000, and 10000 Å and a linear column with mixed pore sizes were used. The total molecular weight of the rod–coil block copolymer was found to be 135 000 (relative to a PS standard in THF) and the weight fraction of PS about 0.20. GPC in THF yielded a polydispersity of 1.36.

III. Experimental Section

Several experimental techniques were used to study and characterize the P(S-*b*-HIC) rod–coil block copolymer. Optical microscopy (OM) of concentrated sheared and unsheared block copolymer solutions was performed under crossed polarizers to investigate the liquid crystalline behavior of the diblock as compared with the homopolymer.[34,35] Optical micrographs were taken at magnifications of 10× and 32× using a Carl–Zeiss Axioskop. Samples were prepared by placing small drops of a concentrated (~5 wt %) solution in CCl_4 onto glass slides, and shearing was accomplished with a razor blade.

Bright field transmission electron microscopy (TEM) using a JEOL 200CX was used to study the microphase-separated morphology of both bulk films and thin films. Bulk samples used for cross-sectional TEM were slow cast from 5 wt % solutions in toluene onto epoxy plugs for 5 days. After reembedding in epoxy, the plugs were microtomed at room temperature using a Reichert-Jung FC-4E ultramicrotome. The approximately ~500 Å sections were floated in distilled water onto copper grids and stained in RuO_4 vapors for 5 min. Thin film samples of P(S-*b*-HIC) were cast from dilute 0.05 wt % solutions in toluene, CCl_4, and $CHCl_3$ onto carbon-coated mica sheets using a micropipet and allowed to solvent anneal for 1 day in a solvent saturated environment. The thin carbon-supported films were then floated off on distilled water and picked up on copper grids which were stained in RuO_4 vapors for 2.5–7.5 min. In addition to TEM, electron diffraction (ED) was used to study both the orientation of the rods with respect to the microphase-separated microstructure and the crystal structure of the rod block in the thin film samples.

X-ray diffraction using a Rigaku RU-300 rotating anode diffractometer and wide angle X-ray scattering (WAXS) using a sealed tube Enraf Nonius Diffractis 583 X-ray generator employing 1.54 Å Cu Kα radiation was performed to verify and provide further information for the crystal structure analysis of the PHIC block. Films ~1 mm thick for X-ray diffraction were slow cast from 5 wt % solutions in toluene for 1 week. P(S-*b*-HIC) fibers for WAXS were prepared by first heating a few drops of a 5 wt % solution in toluene to ~100 °C on a hotplate. After most of the solvent had evaporated, tweezers were then used to pull small fibers from the remaining melt.

IV. Results and Discussion

Figure 2 shows the optical micrograph of a concentrated (>15 wt %) solution of the P(S-*b*-HIC) viewed at 32× under crossed polarizers. Light is transmitted through the solution because its state of polarization is altered by the birefringent P(S-*b*-HIC) domains, thereby resulting in a fraction of the light polarized parallel to the analyzer. The micrograph clearly shows that the

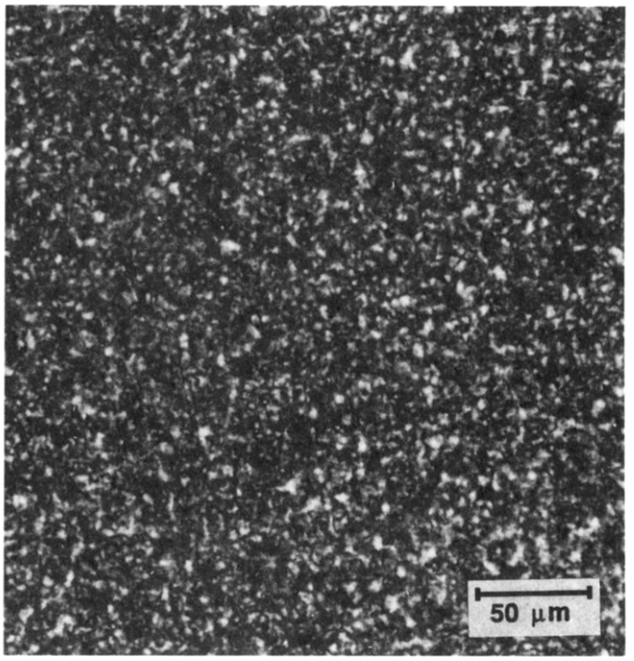

Figure 2. Optical micrograph, employing crossed polarizers, of a concentrated (>15 wt %) solution of P(S-*b*-HIC). The nonuniform birefringent pattern is due to the random orientation of the ~5 μm liquid crystalline regions.

diblock copolymer solution is birefringent and consists of numerous liquid crystalline regions which are at least 5 μm in size and are randomly oriented. In contrast, Figure 3A shows an optical micrograph of the same solution after it was sheared by a razor blade and allowed to relax before eventually becoming a solid film. The characteristic banded texture, which has been observed previously in optical microscopy studies of sheared solutions[35] and drawn samples[31] of PHIC, is oriented perpendicular to the shearing direction indicated by the arrow. When rotated under crossed polarizers, the transmitted light in any given band alternates in a periodic light-gray–dark-gray sequence. Assuming the optic axis is along the PHIC chain axis, Figure 3B shows a schematic model depicting the local director field of the P(S-*b*-HIC) molecules across the shear band texture which successfully explains the OM results. The model consists of alternating ~3 μm thick bands in which the director field of adjacent bands is oriented either +22 or −22° to the shear direction. To explain the finer details seen in the optical microscope, the model also incorporates a thin transition region between the large bands in which the molecules are aligned parallel to the shear direction. The OM results clearly show that the rod–coil diblock copolymer behaves mesogenically on the micron length scale despite the presence of the PS coil block.

While OM shows that P(S-*b*-HIC) does not behave at all like a typical coil–coil diblock on the macroscopic scale, it does not give any structural information about P(S-*b*-HIC) on the microscopic scale. TEM was used to study the fine scale morphology. Figure 4 shows the cross-sectional bright field TEM micrograph obtained from a bulk sample of P(S-*b*-HIC) cast from toluene, a preferential solvent for PS. The dark regions are the PS domains which have been preferentially stained with RuO_4 and the lighter regions are the unstained PHIC domains. At first glance, the alternating layers of PS and PHIC appear as lamellae. However, closer inspection of the micrograph shows that the PS and PHIC

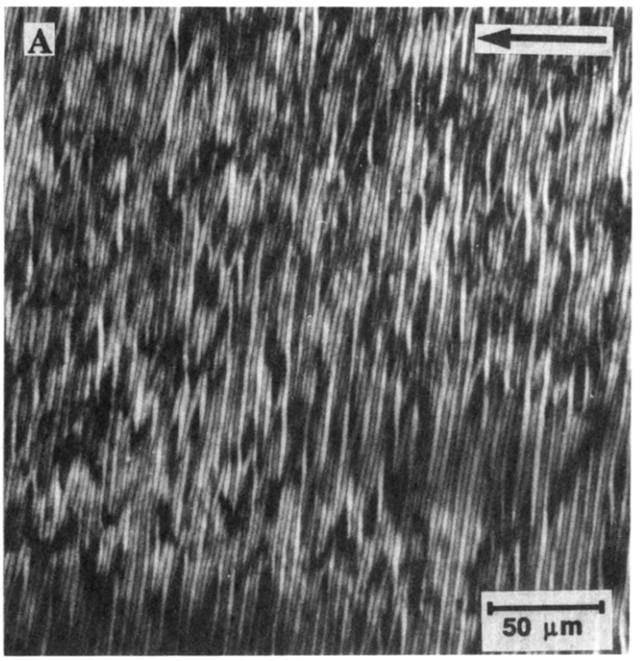

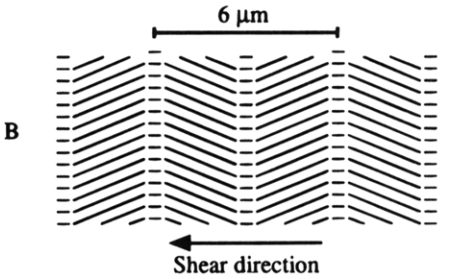

Figure 3. (A) Optical micrograph, employing crossed polarizers, which shows the banded texture that results after a concentrated (>15 wt %) solution of P(S-*b*-HIC) is allowed to relax after being sheared. The shear direction is indicated by the arrow. The bands are ~3 μm in size. (B) Schematic diagram of the liquid crystalline banded texture resulting from the relaxation of the P(S-*b*-HIC) solution after being sheared. The diagram illustrates the local director field of the PHIC rod block across the bands. The director field in adjacent bands is oriented either +22° or −22° to the shear direction. A thin transition region in which the rod director is parallel to the shear direction is located between the bands.

layers form "zigzags" which are correlated spatially. In this zigzag lamellar structure, the PS domains have a width of approximately 200 Å while the PHIC domains range in size from 300 to 1100 Å. The P(S-*b*-HIC) sections, however, were found to be highly beam sensitive in the TEM. At the operating voltage of 200 keV, the electron beam lifetime of the PHIC crystals was about one-third that of a stretch-oriented PE film. Using the known value for the maximum beam dosage of PE at 200 keV and 20 °C, the maximum beam dosage for the PHIC is estimated to be $\sim 4.7 \times 10^{-3}$ C/cm^2. Because the domain spacing may be affected by electron irradiation, the measured domain spacings should only be used as a rough estimate of the actual values.

In an effort to reduce beam damage and also to study the microstructure of the P(S-*b*-HIC) without the problems of projection overlap and sample deformation due to microtoming, thin film samples of the P(S-*b*-HIC) cast on carbon support films were prepared and studied using TEM. Figure 5 shows a bright field TEM micrograph of a thin P(S-*b*-HIC) film cast from a toluene solution. The micrograph clearly shows the periodic

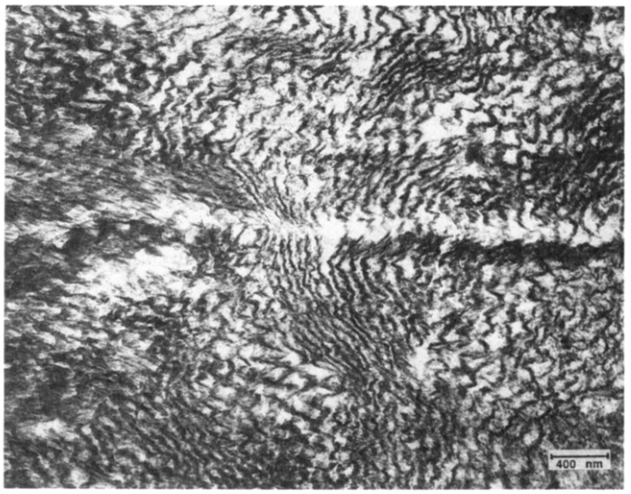

Figure 4. Cross-sectional bright field TEM micrograph of a bulk film cast from toluene. The micrograph shows the zigzag microphase-separated morphology in which the lighter regions are the PHIC domains and the darker regions are the RuO_4-stained PS domains.

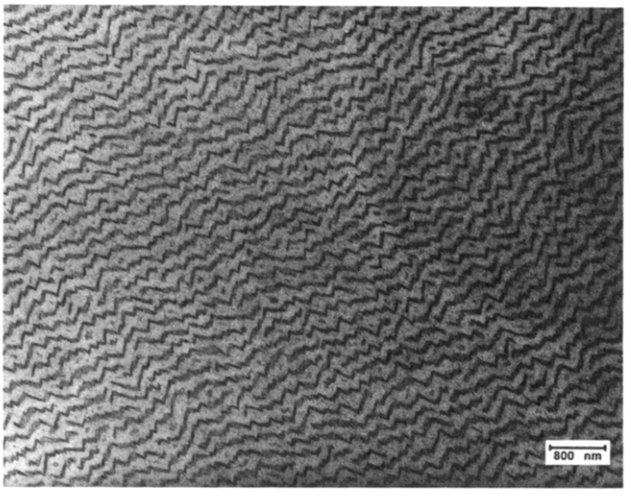

Figure 5. Bright field TEM micrograph of a thin film cast from toluene. The micrograph shows the zigzag morphology, which possesses long range smectic-like order and a high degree of spatial correlation between adjacent layers.

zigzag morphology (in agreement with the cross-sectional TEM results) of the rod−coil diblock which possesses long range smectic-like order and a high degree of spatial correlation between adjacent layers. The dark and light areas which correspond to the PS and PHIC domains have average domain spacings of ~250 and ~1800 Å, respectively. The variation in domain size of the PS layers over the image is most likely a projection artifact due to a slight tilt of the PS zigzags which are oriented on average perpendicular to the substrate. The discrepancy of the PHIC domain size between the bulk and thin films, however, may be due to large film shrinkage of the unsupported bulk sections resulting from mass loss due to electron beam scission of the PHIC. In comparison, the thin films are dimensionally more stable because of the carbon substrate. From the micrograph, a number of important observations can be made about the zigzag morphology. First, the unique zigzag ordering of the P(S-*b*-HIC), which has not been observed before in coil−coil or rod−coil block copolymers, can only be a result of the liquid crystalline and or crystalline order of the rodlike PHIC block. Second, from the global orientation of all the zigzags,

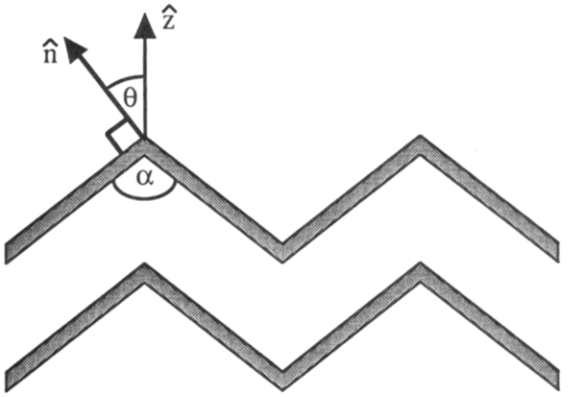

Figure 6. Schematic diagram of the lamellar zigzags. The figure shows the zigzag direction $\hat{\mathbf{z}}$, lamellar normal $\hat{\mathbf{n}}$, and the zigzag angle α.

Figure 7. Wide angle electron diffraction pattern of an unstained thin film cast from toluene. The large number (21) of reflections indicates a high degree of crystallinity in the PHIC domains while the narrow azimuthal breadth indicates very high orientational order over the 2 μm diameter region used for diffraction.

one can see that the PHIC rods strongly interact with each other analogous to what happens in a nematic or smectic liquid crystal. And third, the angle between zigzags which we denote by α (see Figure 6) can be seen to be fairly constant at an average value of ~90°.

To determine the orientation of the PHIC rod block with respect to the zigzag lamellae and also to get a better idea of the type of ordering present in the PHIC domains, wide angle electron diffraction was performed on the sample cast from toluene. Figure 7 shows a representative electron diffraction pattern resulting from an area similar to that shown in Figure 5. The electron diffraction pattern exhibits apparent fiber symmetry which shows that, in addition to being orientationally ordered on the molecular scale, the PHIC domains are crystalline. In addition, the large number (21) of reflections (a schematic diffraction pattern is shown in Figure 8) indicates that the degree of crystallinity is high. To the best of our knowledge, a full crystal structure determination of PHIC has never been performed. As mentioned earlier, however, WAXS of unoriented and drawn samples of PHIC was done by

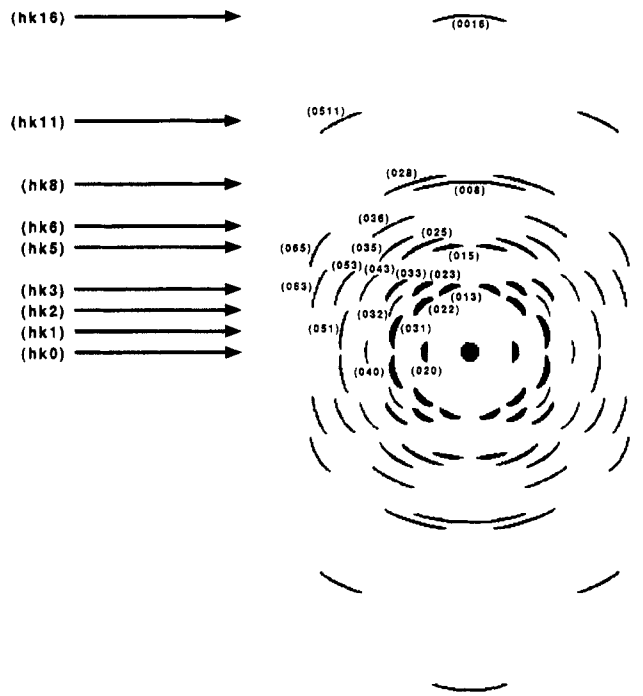

Figure 8. Indexed schematic diagram of the wide angle electron diffraction pattern from a thin P(S-*b*-HIC) film cast from toluene. All reflections are of the (0*kl*) type. The first meridional reflection is the (008).

Clough.[31] From his data, he concluded that the PHIC chains adopted a 12_5 helix with a two monomer repeat unit of 3.1 Å. In addition, he found that crystallization from toluene and THF resulted in two different sets of *d* spacings, indicating polymorphism although no unit cells were proposed. As a result, an analysis of the ED patterns (a representative ED pattern is shown in Figure 7) was undertaken. The presence of meridional reflections indicated that in the unit cell the *c* axis was perpendicular to the *a* and *b* axes. By measuring the vertical spacing of the layer lines on the ED pattern, the *c* axis repeat distance was calculated to be $c = 15.6$ Å. Further analysis of the two equatorial reflections and the other layer line reflections revealed that the ED pattern could be successfully indexed entirely with (0*kl*) type reflections. As a result, only information in two directions of reciprocal space was present in the ED patterns. Consequently, aside from *c*, only $b \sin \gamma = 13.08$ Å could be determined. The presence of only (0*kl*) reflections is strongly indicative of a lack of fiber symmetry caused by preferred crystal growth of the PHIC domains on the carbon substrate. Additional evidence for preferred crystal growth is provided by ED experiments which showed additional equatorial reflections when the sample was tilted about the *c* axis.

WAXS of P(S-*b*-HIC) drawn fibers and X-ray powder diffraction of a bulk sample cast from toluene were performed to determine the remaining unit cell parameters and conclusively show whether the thin film samples exhibit a preferred crystal orientation. While the degree of orientation was only moderate, the WAXS pattern of the fiber sample did exhibit fiber symmetry and showed five equatorial reflections. The additional equatorial reflections confirm that the PHIC domains in the thin samples are oriented with the (010) planes normal to the substrate. Excluding the first reflection, dividing the remaining equatorial Bragg spacings by the second Bragg spacing resulted in the $1:3^{1/2}:4^{1/2}:7^{1/2}$ ratios expected for hexagonal packing of the rods, which disagrees with the *d* spacings reported by Clough. The first reflection, which has a *d* spacing of ~15.8 Å and whose intensity is minor relative to the second reflection, may be attributable to another crystal structure. Using the WAXS data, the remaining unit cell parameters were calculated from the ED data to be $a = b = 15.1$ Å and $\gamma = 120°$. The crystal density of PHIC was calculated to be 1.10 g/cm^3 for a unit cell containing two molecules, which agrees well with the experimentally measured[35] value of 1.00 g/cm^3. Although the WAXS data suggest hexagonal packing of the rods, the X-ray powder diffraction profile obtained from the bulk film cast from toluene showed several reflections which could not be indexed according to a hexagonal unit cell. These results support Clough's findings of polymorphism in PHIC.

In addition to crystal structure information, valuable information on the molecular conformation of the PHIC rods was obtained by analyzing the diffracted intensity corresponding to each layer line of the ED pattern. From helical diffraction theory, the equation

$$l = tn + um \tag{1}$$

for a u_t helix (*t* turns for *u* units) can be derived where *n* and *m* are integers and *l* is the layer line. Solutions of eq 1 give the orders, *n*, of the Bessel functions which contribute to the helix structure factor on the *l*th layer line. Layer lines with low-order Bessel functions, such as $n = 0$, 1, or 2, are expected to have strong intensity reflections. According to Clough, high-intensity reflections for PHIC were observed on the $l = 0$, 2, 5, 7, and 12 layer lines, which agrees with the intensity distribution predicted by eq 1 for a 12_5 helix. This intensity distribution, however, is not at all consistent with the layer line intensities observed from the P(S-*b*-HIC) ED patterns. As a result, the intensity distributions for other helices were calculated and compared to the ED patterns. Table 1 shows the list of Bessel functions which contribute to each layer line for an 8_3 helix generated using eq 1. The intensities resulting from an 8_5 helix are identical to those of an 8_3 helix because the helices differ only in their respective handedness. Inspection of Table 1 shows that out of the first eight layer lines, the $l = 0$, 3, 5, and 8 layer lines will have the strongest reflections. Figure 8 shows strong reflections on the $l = 3$ and 5 layer lines which are characteristic of first-order Bessel functions in agreement with Table 1. In addition, meridional reflections are only allowed on the layer lines that are integer multiples of eight because of the zero-order Bessel functions, which is confirmed by the presence of the (008) and the (0,0, 16) reflections. The 1.95 Å *d* spacing obtained from the (008) reflection yields L_o, the projection of the intermonomer distance onto the major axis of the helix, which is in good agreement with the previously published values of 1.8−2.0 Å.[37,38] As a result, the PHIC block can be assigned a conformation of either an 8_3 or 8_5 helix which have a translation of 1.95 Å and rotation of 135° per monomeric unit along the *c* axis. The same 8_3 helical conformation was found by Shmueli et al. using X-ray diffraction on oriented poly(*N*-butyl isocyanate) films.[39] A subsequent qualitative fit of the predicted Bessel function structure factors for an 8_3 or 8_5 helix to the measured intensity distributions of each layer line using the PHIC helix radius as a fitting parameter yielded a radius of ~3.25 Å. The equatorial reflections indicate hexagonal packing of the chains which suggests a two chain monoclinic or triclinic (pseudohexagonal) unit cell for crystalline PHIC.

Table 1. List of Bessel Functions Which Contribute to Each Layer Line for an 8_3 Helix Generated Using Equation 1

l	n	m	n	m	n	m
0	0	0	8	-3	-8	3
1	3	-1	-5	2		
2	-2	1	6	-2	-10	4
3	1	0	-7	3	9	-3
4	4	-1	-4	2		
5	-1	1	7	-2	-9	4
6	2	0	-6	3	10	-3
7	-3	2	5	-1		
8	0	1	8	-2	-8	4
9	3	0	-5	3		
10	-2	2	6	-1	-10	5
11	1	1	-7	4	9	-2
12	4	0	-4	3		
13	-1	2	7	-1	-9	5
14	2	1	-6	4	10	-2
15	-3	3	5	0		
16	0	2	8	-1	-8	5

Besides providing structural and conformational information, electron diffraction also showed how the PHIC chains were oriented with respect to the zigzags. Figure 12B shows the defocused (000) bright field image of a similar toluene cast thin film superimposed on its respective electron diffraction pattern. Since there is no relative rotation (see Figure 12C) between the diffraction pattern and the bright field image in this mode of operation, the micrograph clearly shows that the chain axis of the PHIC rods is oriented parallel to the direction in which the zigzags point which we denote by $\hat{\mathbf{z}}$ (see Figure 6).

Using the information obtained from the TEM and ED data, a model showing how the P(S-*b*-HIC) chains pack in the zigzags was constructed. Figures 9A and 9B show schematic drawings of two possible chain packing arrangements of the zigzag microstructure. The zigzag direction $\hat{\mathbf{z}}$ and angle α are also pictured. The important feature present in both the interdigitated and the bilayer model is that the PHIC rods are tilted with respect to the interface separating the PS and the PHIC domains. While tilt of the rodlike block has been theoretically predicted for rod−coil block copolymers[20−23] and observed in a polypeptide rod-coil block copolymer,[22] this work represents the first direct observation of this effect in a synthetic nonbiological rod−coil block copolymer. The reasons for the tilt can be understood by considering the thermodynamics of chain packing in single rod−coil lamellae.

Following the treatment given by Halperin, we consider a single perfectly flat lamellae formed by aggregation of the rod−coil block copolymer in a solvent preferential to the coil block. The AB rod−coil block copolymer consists of N_A rod monomers chemically connected to N_B coil monomers at a single covalent junction. In addition, because the A block is a rigid rod,

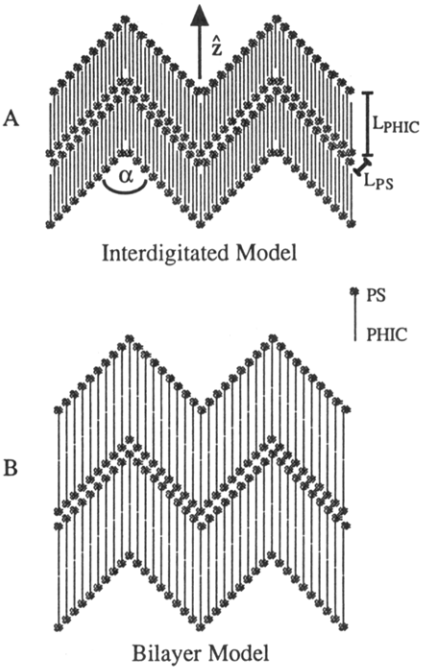

Figure 9. (A) Schematic diagram depicting the packing arrangement of the chains in the zigzag morphology in which the PHIC rods interdigitate. (B) Schematic diagram depicting the packing arrangement of the chains in the zigzag morphology in which the block copolymer molecules order in a bilayer.

its length L which scales linearly with N_A is much greater than its width, d. The isolated lamellae is made up of three layers, a central rod layer and two exterior coil layers. In the central layer, the rods pack together to minimize unfavorable enthalpic contacts with the coil block and the preferential solvent and are aligned along a local director. Since the solvent is preferential, the AB junctions are expected to be well localized between the adjacent rod and coil domains, giving rise to a narrow interface which is characterized by a small area per junction. As a result, in the outer layers, the coils form stretched swollen brushes which are tethered to the rods. In such a system, two terms are expected to contribute to the free energy per chain, namely $F_{\text{interface}}$ and $F_{\text{deformation}}$. $F_{\text{interface}}$ is an enthalpic term which takes into account the surface free energy resulting from the interface between the rods and the solvent swollen coils. While $F_{\text{deformation}}$ is an entropic term which takes into account the elastic deformation of the coils. Assuming that the rods are oriented normal to the rod−coil interfaces, Halperin derived the following expressions for $F_{\text{interface}}$ and $F_{\text{deformation}}$:

$$F_{\text{interface}} \sim \gamma d^2 \tag{2}$$

$$F_{\text{deformation}} \sim N_A (a/d)^{5/3} kT \tag{3}$$

In the above expressions, γ and a are the surface tension of the rod−solvent/coil interface and the characteristic size of a B coil monomer, respectively. When the rods of the central layer are allowed to tilt an angle θ with respect to the lamellar normal (see Figure 10), two things occur. First, because tilt exposes some new area of the rods to the coil and solvent, the amount of rod surface area contributing to $F_{\text{interface}}$ increases. Second, because the tilt causes the rod−coil junctions to spread apart, the area per chain increases and the degree of coil stretching is reduced which lowers $F_{\text{deformation}}$. As a result, $F_{\text{interface}}$ and $F_{\text{deformation}}$ need to be

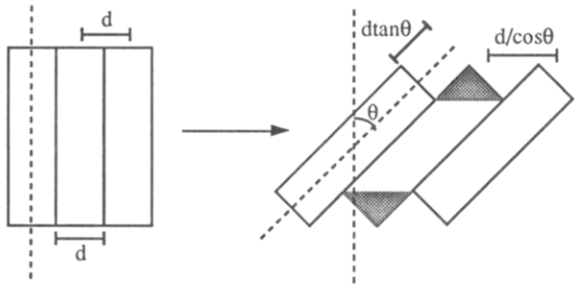

Figure 10. Diagram (adapted from ref 26) showing the effect of rod tilt on the interfacial area and the average separation between junctions. The shaded area indicates the new surface exposed to the solvent after tilt.

modified by geometrical factors. The resulting general form of the free energy per chain is

$$F \sim \gamma d^2(1 + \tan\theta) + N_A(a/d)^{5/3}kT(\cos\theta)^{5/6} \quad (4)$$

Equation 4 can be rewritten in terms of a parameter δ that is equal to the ratio $F_{\text{interface}}(\theta=0)/F_{\text{deformation}}(\theta=0)$ and which characterizes the phase behavior of the rod−coil system. Halperin found that for $0 < \delta < \sim 1/4$, $F_{\text{deformation}}$ dominates and a tilted smectic C phase is found to be more stable. For $\delta > \sim 1/3$, $F_{\text{interface}}$ dominates and the untilted smectic A phase results in the minimum free energy per chain.

While the thermodynamic theory presented above is strictly valid only for a single rod−coil lamellar sheet, it captures the essential underyling physics governing the phase behavior of the P(S-*b*-HIC) rod−coil. In solution, tilt of the PHIC rods occurs because it minimizes the energetic penalties associated with chain deformation of the PS coil block and the interfacial tension resulting from the incompatibility between the PHIC block and the PS block. Chain tilt is also well-known for chain-folded homopolymers[41] and amorphous coil/crystalline chain-folded block copolymers[42] because it relieves overcrowding at the crystal surface. An examination of Figure 10 shows that a tilt of the rod blocks is also equivalent to a successive translation along the rod chain axis between adjacent rods. Furthermore, it can be seen that translation along the chain axis in either direction results in a reduction in the free energy of stretching for the coil block. As a result, it is equally probable for the rods to translate in either direction along the chain axis thereby giving rise to zigzags. As the solvent evaporates, the coils become less swollen and the tilt angle θ decreases continuously. The theory, however, eventually breaks down when the solution becomes too concentrated and the PHIC crystallizes. At this point, the tilt angle and actual distance of the translation of the PHIC rods cannot be determined by the above thermodynamic arguments. Instead, an even stronger driving force dictates what translation distances and tilt angles are selected. Namely, PHIC is three-dimensionally *crystalline*, as shown by ED. In order to preserve the crystal structure and avoid a large lattice strain energy penalty, the translation of adjacent unit cells is constrained to be nc where n is an integer and c is the c axis repeat distance of the unit cell (see Figure 11). As a result, the allowed tilt angle θ becomes quantized. Once crystallization of the PHIC rods occurs, the rods lock into the nearest allowed tilt angle. Using the lattice constants of the pseudoehxagonal unit cell and the fact that the PHIC domains are preferentially oriented with the (010) planes normal to the substrate, the tilt angle

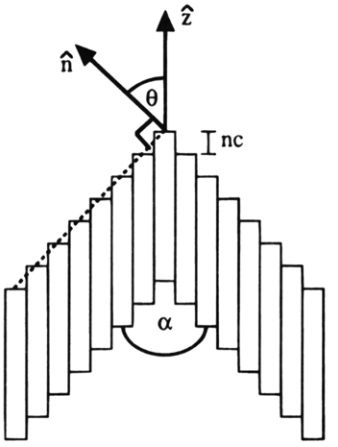

Figure 11. Diagram showing the quantization of the tilt angle θ and the zigzag angle α resulting from crystallization of the rods. The tilt and zigzag angles are quantized because the translation of adjacent unit cells along the chain axis must be an integral number of the c axis repeat distance.

is θ = 45.9, 64.2, and 72.1° for n = 1, 2, and 3, respectively. The predicted tilt angle, $\theta = 45.9°$, which is most consistent with the TEM results, yields $\alpha = \pi - 2\theta = 88.1°$. This value agrees well with the experimentally observed zigzag angles which range from 67 to 105°.

Of the two proposed models for the zigzag morphology, the interdigitated model is more consistent with domain spacing predictions based on molecular weight data. In the zigzag microstructure (see Figure 9A), the PS domain spacing L_{PS} is expected to scale with the molecular weight to a power greater than the $^2/_3$ power because the coils are highly stretched away from the rods. To get an estimate for the PS domain spacing, an experimentally calculated expression for the lamellar repeat distance of a symmetric P(S-*b*-2VP) diblock copolymer in the strong segregation limit was used.[40] Using an approximate value for the PS molecular weight of 30 000, the PS domain size was calculated to be about 190 Å assuming a bilayer. While only approximate, the predicted PS domain spacing is quite close to domain spacings measured from TEM micrographs which were about 200 Å. In contrast, the PHIC domain size L_{PHIC} is expected to scale linearly with the PHIC molecular weight (see Figure 9A). Using a molecular weight for the PHIC block of about 110 000 and a monomer repeat distance measured from ED to be 1.95 Å, L_{PHIC} was calculated to be about 1700 Å for the interdigitated model. This domain spacing is in reasonable agreement with the average value obtained from TEM micrographs of about 1800 Å, which suggests that the PHIC rods are indeed interdigitated in the zigzag morphology. Intuitively, one would expect interdigitation because it helps further reduce the chain stretching of the coil block by increasing the distance between junctions by a factor of 2 and the area per junction by a factor of 4.

So far, the discussion of the zigzag morphology has centered around the thin film and bulk samples cast from toluene, a solvent which is preferential to the PS block. In order to study the role of solvent in the resultant microstructure of the P(S-*b*-HIC) system, the morphology of the rod−coil was studied in samples cast from two other solvents. Figures 12A, 13, and 14 show characteristic bright field TEM micrographs obtained for thin film samples cast from toluene, CCl_4, and $CHCl_3$, respectively. Figure 12B also shows the electron

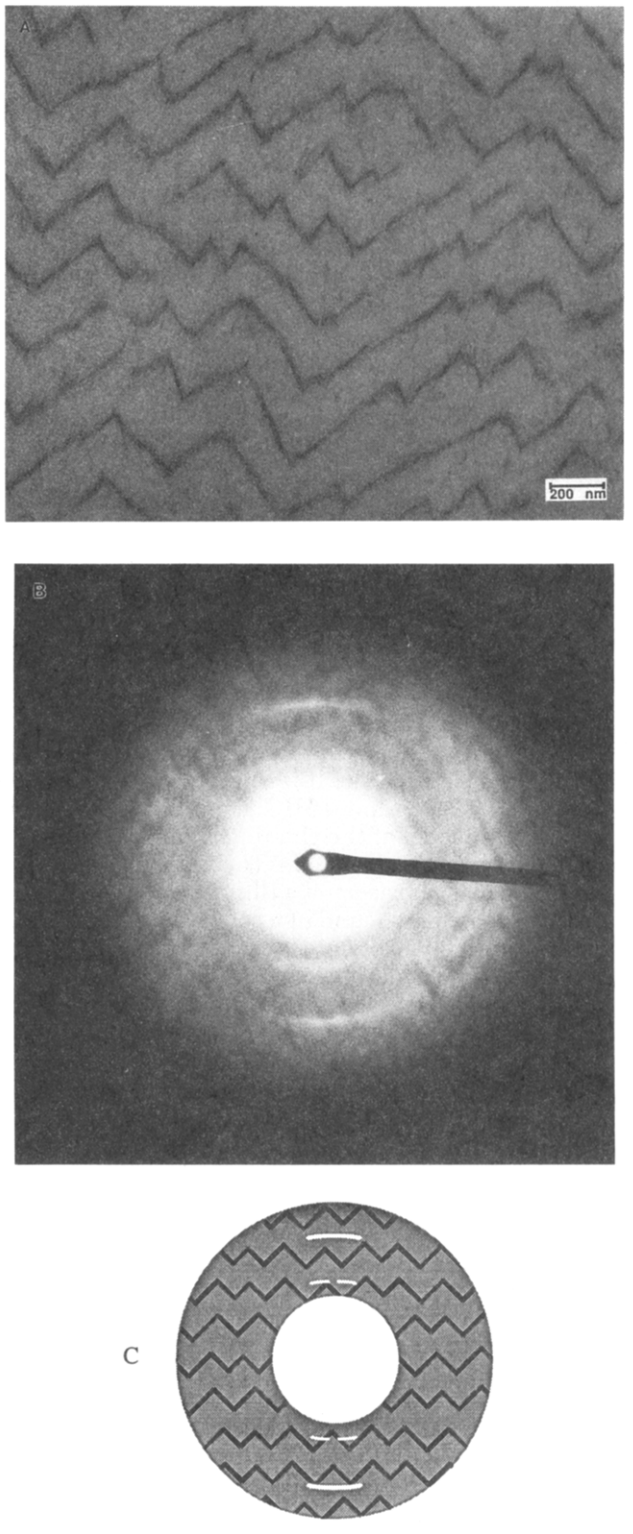

Figure 12. (A) Bright field TEM micrograph of a thin film cast from toluene. The micrograph shows that the zigzag morphology exhibits long range order and a high degree of correlation between adjacent zigzag layers. (B) Superimposed electron diffraction pattern and defocused (000) bright field image of an area similar to Figure 11A. The pattern shows that the chain axis of the PHIC rods is parallel to $\hat{\mathbf{z}}$ and that the PHIC domains are highly crystalline. (C) Schematic diagram of Figure 12b which shows the superimposed electron diffraction pattern and defocused (000) bright field image of the zigzag morphology.

diffraction pattern for the toluene sample superimposed on the defocused (000) bright field image. As described earlier, the toluene cast sample exhibits long range order and a high degree of spatial correlation between adjacent zigzags in the plane of the film. The diffraction pattern also shows that the crystalline PHIC domains are highly oriented throughout the sample. In contrast, the morphology exhibited by the CCl_4 sample consists of highly fragmented PS zigzags which are surrounded by a crystalline PHIC matrix which lacks long range orientational order. As a result, diffraction patterns of the CCl_4 samples clearly show rings indicating a random orientation of the PHIC domains in the plane of the film. Numerous dark regions corresponding to PS domains whose two-dimensional projection varies from circular to elongated are also present within the PHIC matrix. These regions resemble PS micelles. The sample cast from $CHCl_3$ shows a morphology consisting of short zigzags in which the orientation of adjacent PHIC domains in the plane of the film is weakly correlated. As expected, the corresponding diffraction patterns consist of broad arcs. The micelle-like PS regions observed in the CCl_4 samples are also present in the $CHCl_3$ samples.

As observed, solvent quality significantly affects the morphology formed by the P(S-*b*-HIC) in the solid state. The initial state of the rod–coil chains in the three

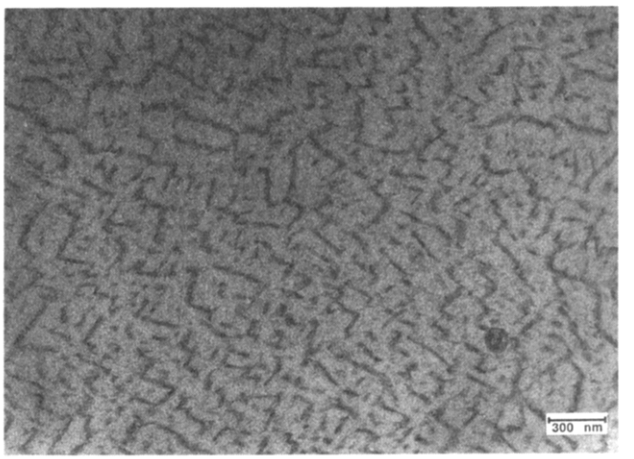

Figure 13. Bright field TEM micrograph of a thin film cast from CCl_4. The micrograph shows that the microphase-separated morphology consists of fragmented PS zigzags surrounded by a crystalline PHIC matrix which lacks long range orientational order. Numerous PS inclusions are also present throughout the PHIC matrix which resemble micelles.

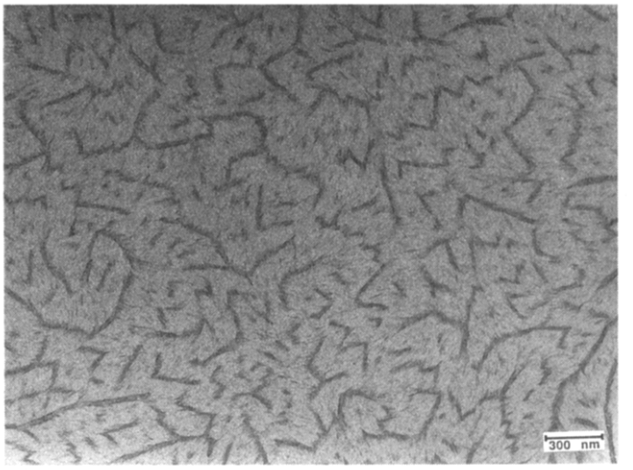

Figure 14. Bright field TEM micrograph of a thin film cast from $CHCl_3$. The micrograph shows that the microphase-separated morphology consists of short zigzags in which the adjacent domains are weakly correlated. Numerous PS inclusions are also present throughout the PHIC matrix which resemble micelles.

solvents was nearly identical because all three samples were cast from isotropic solutions. However, because the resulting morphologies in the solid state were quite different, the three intervening paths by which the rod–coil block copolymers self-assembled must be different. As evaporation proceeds, both macrophase separation of the solution and microphase separation of the rod–coil diblock occur. The choice of solvent most likely determines what phases macrophase separate from the isotropic solution before microphase separation of the rod–coil and crystallization of the PHIC take place. In particular, solvent can be thought to influence microphase and macrophase separation in the following two ways. First, the intermolecular interactions between the PHIC rods, which control the liquid crystalline ordering of the rod block, are screened to a different extent depending on the solvent. And second, the relative importance of interfacial energy to coil deformation in the free energy is solvent dependent through changes in the surface tension γ and the extent to which the solvent swells the PS block. Consequently, three different paths can be proposed to explain the final morphologies observed in the three samples.

For the toluene sample, solvent evaporates until v_c of P(S-*b*-HIC) is reached, at which point the solution macrophase separates into an isotropic solvent rich phase and a nematic rod–coil rich phase. As the interaction between rods becomes stronger, the rod–coil chains may microphase separate and undergo a second transition to a smectic phase. The preferential swelling of the PS domains by the toluene increases chain stretching and provides the driving force for rod tilt and formation of the zigzag morphology. After further evaporation, the PHIC rods eventually crystallize, locking in the well-ordered long range zigzag microstructure. In contrast, CCl_4 is a nonpolar solvent which is preferential for the PHIC block. In this case, as the solvent evaporates, the solution could undergo liquid–liquid phase separation into an isotropic solvent rich phase and a rod–coil rich isotropic phase. As the solvent evaporation continues, the preferential swelling of the PHIC most likely hinders the formation of any liquid crystalline phases before crystallization occurs. In addition, because the PS coils are not swollen, the chain stretching of the coil block is somewhat relieved, reducing the driving force for rod tilt. Consequently, the observed morphology consists of numerous PS micelle-like inclusions and very few zigzags in which the PHIC crystalline domains making up the matrix are randomly oriented. Compared to toluene and CCl_4, the polar solvent $CHCl_3$ is not significantly preferential for either block. As a result, as the solvent evaporates, macrophase separation of the isotropic solution and microphase separation of the rod–coil diblock may occur at about the same time, resulting in a solvent-rich isotropic phase and a rod–coil rich smectic phase. The microphase separation of P(S-*b*-HIC) directly into a smectic phase bypassing a nematic phase limits any long range order. In addition, compared to the toluene sample, the nonpreferential nature of $CHCl_3$ results in less coil stretching and a smaller driving force for rod tilt. Finally, crystallization of the PHIC eventually occurs and locks in the morphology. As a result, the observed morphology shows a frustrated zigzag microstructure. On the length scale of the PHIC block, tilting of the rods can be seen and short range zigzags are apparent. But on a larger length scale, individual PHIC domains are uncorrelated, resulting in fragmentation of the PS domains. The possible paths discussed above appear consistent with the observed end state morphologies.

V. Summary

A model P(S-*b*-HIC) rod–coil block copolymer was synthesized and used to investigate the morphology and phase behavior of rod–coil diblock copolymers. The structure was characterized with optical microscopy, transmission electron microscopy, electron diffraction, and wide angle X-ray diffraction. OM confirmed that the rod–coil block copolymer exhibited liquid crystalline behavior similar to that observed for the homopolymer PHIC. TEM of bulk and thin film samples cast from toluene solutions showed the presence of a novel zigzag morphology. This morphology was found to consist of alternating PS and PHIC zigzag layers which possess smectic-like long range order. ED of thin film samples showed that the PHIC domains were highly crystalline and oriented with the (010) planes normal to the substrate. The ED data, together with WAXS patterns of drawn P(S-*b*-HIC) fibers, showed that the PHIC rods adopted either an 8_3 or 8_5 helix and packed in a monoclinic or triclinic (pseudohexagonal) unit cell. The unit cell, which contains two chains, has the lattice constants $a = b = 15.1$ Å, $c = 15.6$ Å, and $\gamma = 120°$. In addition, ED data which showed the orientation of the PHIC rods with respect to the zigzags confirmed that the rods were tilted with respect to the interface separating the PS and PHIC domains. From this knowledge, a model of the chain packing in the zigzag morphology was constructed. Theoretical arguments based on Halperin's theory of a tilting transition in rod–coil block copolymers found in a solvent preferential for the coil intuitively explain why the zigzag morphology forms. The zigzag morphology is seen to minimize the energetic penalties associated with chain stretching of the coil block and interfacial energy resulting from the interfaces separating the PS and PHIC domains. However, for the solid state morphology of P(S-*b*-HIC), the theory must be modified to take into account crystallization of the rod block, which causes the allowed tilt angle to be quantized. Predictions for the domain spacings and zigzag angle are consistent with values obtained from TEM. Finally, the phase behavior of the P(S-*b*-HIC) rod–coil was studied by casting thin films from solutions in toluene, CCl_4, and $CHCl_3$ and examining the resultant solid films with TEM and ED. The three solutions yielded significantly different morphologies ranging from well-ordered zigzags to highly fragmented zigzags in which the PHIC domains were randomly oriented in the plane of the film. In addition, the PHIC matrix of the CCl_4 and $CHCl_3$ samples contained PS regions which resembled micelles. The choice of solvent most likely determines what phases macrophase separate from the isotropic solution before microphase separation of the rod–coil and crystallization of the PHIC take place.

Acknowledgment. This work was supported by National Science Foundation Grants DMR90-22933 and DMR92-01845. We are also grateful to Stephanie Simmons and Tim Bunning, who helped in the X-ray diffraction and WAXS experiments, to Guo-Ping Mao for additional characterization of the P(S-*b*-HIC) block copolymer, and to Ted Atkins for useful discussions.

References and Notes

(1) Molau, G. E. In *Block Copolymers*; Aggarwal, S. L., Ed.; Plenum Press: New York, 1970.

(2) Hashimoto, T.; Shibayama, M.; Kawai, H. *Macromolecules* **1980**, *13*, 1237.
(3) Hashimoto, T.; Fujimura, M.; Kawai, H. *Macromolecules* **1980**, *13*, 1660.
(4) Hashimoto, T.; Shibayama, M.; Kawai, H. *Macromolecules* **1983**, *16*, 1093.
(5) Thomas, E. L.; Alward, D. B.; Kinning, D. J.; Martin, D. C.; Handlin, D. L.; Fetters, L. J. *Macromolecules* **1980**, *19*, 2197.
(6) Hasegawa, H.; Tanaka, K.; Yamasaki, K.; Hashimoto, T. *Macromolecules* **1987**, *20*, 1651.
(7) Meier, D. J. *J. Polym. Sci., Part C* **1969**, *49*, 361.
(8) Helfand, E. *Macromolecules* **1975**, *8*, 552.
(9) Helfand, E.; Wasserman, Z. R. *Macromolecules* **1976**, *9*, 879.
(10) Helfand, E.; Wasserman, Z. R. *Macromolecules* **1978**, *11*, 960.
(11) Helfand, E.; Wasserman, Z. R. *Macromolecules* **1980**, *13*, 994.
(12) Leibler, L. *Macromolecules* **1980**, *13*, 1602.
(13) Ohta, T.; Kawasaki, K. *Macromolecules* **1986**, *19*, 2621.
(14) Semenov, A. N. *Sov. Phys. JETP* **1985**, *61*, 733.
(15) Fredrickson, G. H.; Liu, A. J.; Bates, F. S. *Macromolecules* **1994**, *27*, 2503.
(16) Milner, S. T. *Macromolecules* **1994**, *27*, 2373.
(17) Bates, F. S.; Schultz, M.; Rosedale, J. H.; Almdal, K. *Macromolecules* **1994**, *27*, 2503.
(18) Flory, P. J. *Proc. R. Soc. London, A* **1956**, *243*, 73.
(19) Barenberg, S.; Anderson, J. M.; Geil, P. H. *Int. J. Biol. Macromol.* **1981**, *3*, 82.
(20) Perly, B.; Douy, A.; Gallot, B. *Makromol. Chem.* **1976**, *177*, 2569.
(21) Douy, A.; Gallot, B. *Polym. Eng. Sci.* **1977**, *17*, 523.
(22) Douy, A.; Gallot, B. *Polymer* **1987**, *28*, 147.
(23) Nakajima, A.; Hayashi, T.; Kugo, K.; Shinoda, K. *Macromolecules* **1979**, *12*, 840.
(24) Radzilowski, L. H.; Wu, J. L.; Stupp, S. I. *Macromolecules* **1993**, *26*, 879.
(25) Semenov, A. N.; Vasilenko, S. V. *Sov. Phys. JETP (Engl. Transl.)* **1992**, *62*, 1.
(26) Halperin, A. *Europhys. Lett.* **1989**, *10* (6), 549.
(27) Halperin, A. *Macromolecules* **1990**, *23*, 2724.
(28) Williams, D. R. M.; Frederickson, G. H. *Macromolecules* **1992**, *25*, 3561.
(29) Raphael, E.; de Gennes, P. G. *Physica A* **1991**, *177*, 294.
(30) Raphael, E.; de Gennes, P. G. *Makromol. Chem., Macromol. Symp.* **1992**, *62*, 1.
(31) Clough, S. B. *Characterization of Materials in Research Ceramics and Polymers*; Burke, J. J., Weiss, V., Eds.; Syracuse University Press: Syracuse, New York, 1975; pp 417–436.
(32) Berger, M. N. *J. Macromol. Sci.-Rev. Macromol. Chem.* **1973**, *C9* (2), 269.
(33) Bur, A. J.; Fetters, L. J. *Chem. Rev.* **1976**, *76* (6), 727.
(34) Aharoni, S. M. *Macromolecules* **1979**, *12*, 94.
(35) Aharoni, S. M.; Walsh, E. K. *Macromolecules* **1979**, *12*, 271.
(36) Aharoni, S. M. *J. Polym. Sci., Polym. Phys. Ed.* **1980**, *18*, 1439.
(37) Fetters, L. J.; Yu, H. *Macromolecules* **1971**, *4*, 385.
(38) Berger, M. N.; Tidswell, B. M. *J. Polym. Sci., Part C* **1973**, *42*, 1063.
(39) Shmueli, U.; Traub, W.; Rosenheck, K. *J. Polym. Sci. A* **1969**, *7*, 515.
(40) Matsushita, Y.; Mori, K.; Saguchi, R.; Nakao, Y.; Noda,I.; Nagasawa, M. *Macromolecules* **1990**, *23*, 4313.
(41) Frank, F. C. *Faraday Discuss. Chem. Soc.* **1979**, *68*, 7.
(42) Lotz, B.; Kovacs, A. J.; Bassett, G. A.; Keller, A. *Kolloid-Z. Z. Polym.* **1966**, *209*, 115.

MA941207D